ANL/ET/CP-101735

Creep in Electronic Ceramics*

by

Jules L. Routbort and Kenneth C. Goretta

Energy Technology Division
Argonne National Laboratory
Argonne, IL 60439

Antonio R. de Arellano-Lopez

Departmento de Fisica de la Materia Condensada
Universidad de Sevilla
PO Box 1065
41080 Sevilla, Spain

March 2000

To be presented at Intl. Conf. On Mass and Charge Transport in Inorganic Materials, Venice, Italy, May 28-June 2, 2000.

*Work supported by the U.S. Department of Energy, under Contract W-31-109-ENG-38 and by the Ministerio de Educacion y Ciencias of Spain, under CICYT Project MAT97-1007-C02-01.

DISCLAIMER

DISCLAIMER

Portions of this document may be illegible in electronic image products. Images are produced from the best available original document.

CREEP IN ELECTRONIC CERAMICS*

Jules L. ROUTBORT and Kenneth C. GORETTA

Energy Technology Division, Argonne National Laboratory, Argonne, IL 60439-4838, USA

Antonio R. de ARELLANO–LÓPEZ

Departamento de Fisica de la Materia Condensada, Universidad de Sevilla, P.O. Box 1065, 41080 Sevilla, Spain

High-temperature creep measurements combined with microstructural investigations can be used to elucidate deformation mechanisms that can be related to the diffusion kinetics and defect chemistry of the minority species. This paper will review the theoretical basis for this correlation and illustrate it with examples from some important electronic ceramics having a perovskite structure. Recent results on $BaTiO_3$, $(La_{1-x}Sr_x)_{1-y}MnO_{3+\delta}$, $YBa_2Cu_3O_x$, $Bi_2Sr_2CaCu_2O_x$, $(Bi,Pb)_2Sr_2Ca_2Cu_3O_x$, and $Sr(Fe,Co)_{1.5}O_x$ will be presented.

1. INTRODUCTION

Perovskite–structured ceramics are important technological materials that are finding increasing applications. Applications include, but are not limited to, capacitors, filters, high–current conductors, fuel cells, and membranes. Additionally, some of these materials exhibit extraordinary magnetic properties such as large magnetoresistive responses. Therefore, it is not surprising that there has been a great resurgence of interest in these materials. Microstructural development of ceramics is sensitive to temperature (T) and oxygen partial pressure (PO_2) because processes such as densification and grain growth are diffusion controlled. Therefore, it is important to know, without excessive trial and error, diffusion parameters for successful fabrication of designed microstructures. Measurement of diffusion constants, especially for the rate–limiting species, is complicated because techniques usually involve use of a radioactive tracer and sectioning experiments or, for non-radioactive tracers, use of a profiling technique such as secondary ion mass spectrometry. In the latter case, the penetration depth is small and could even be comparable to or less than a grain diameter.[1,2]

However, deformation studies can yield important and sometimes unique information on the diffusion of the slowest–moving species. Diffusion in a ceramic

* This work was supported by the U.S. Department of Energy, under Contract W–31–109–Eng–38 and by the Ministerio de Educación y Ciencias of Spain, under CICYT Project MAT97–1007–C02–01.

is related to its defect chemistry. Defect concentrations are determined by composition, T, and PO_2. An investigation of the diffusion coefficient as a function of these variables can uniquely identify the diffusing species and its charge state. If a ceramic deforms by a steady–state process under a constant stress (σ), the resulting steady–state strain rate ($\dot{\varepsilon}$) is proportional to the diffusivity of the rate–controlling species. Hence, $\dot{\varepsilon}$ depends uniquely on the composition, T, and PO_2 and can be used to identify the defect. The dependence of $\dot{\varepsilon}$ on PO_2 is often referred to as the defect signature. The steady–state strain rate also depends on σ and is characterized by a stress exponent. The stress exponent is the signature of the deformation mechanism, but it is not sufficient to unambiguously identify the mechanism because several deformation modes predict the same stress exponent. Therefore, it is imperative that deformation studies be accompanied by microstructural observations of the material before and after deformation.

This paper will briefly review the theoretical basis for the formalism that relates steady–state creep to diffusion and defect chemistry. The results will be illustrated by data from several important systems, namely a capacitor material, $BaTiO_3$, a possible air–electrode for a solid–oxide fuel cell, $(La_{1-x}Sr_x)_{1-y}MnO_{3+\delta}$ (LSM), and some layered perovskites, typified by some of the high–temperature superconductors, $YBa_2Cu_3O_x$ (Y123), $Bi_2Sr_2CaCu_2O_x$ (Bi2212), $(Bi,Pb)_2Sr_2Ca_2Cu_3O_x$ (Bi2223), and a candidate oxygen membrane material, $Sr(FeCo)_{1.5}O_x$ (SFC).

2. ANALYSIS OF CREEP DATA

Steady–state deformation is by definition independent of path. That is, a constant–stress creep test performed at σ will yield a steady–state $\dot{\varepsilon}$ and conversely, a constant–strain–rate test performed at $\dot{\varepsilon}$ will yield the same σ. The results can usually be described by the phenomenological equation

$$\dot{\varepsilon} = A\sigma^n D_{eff}, \tag{1}$$

where A is a constant that depends on the details of the mechanism, n is the stress exponent, also dependent on the deformation mechanism, and D_{eff} is the effective diffusion constant.[3]

In fine–grained polycrystalline electronic ceramics, the most commonly reported creep mechanisms are grain–boundary sliding,[4] Nabarro–Herring creep,[5,6] or Coble creep.[7] In all of these cases, Eq. 1 can be modified as

$$\dot{\varepsilon} = BD_{eff}\sigma\Omega / L^2 kT, \tag{2}$$

where B is a constant, Ω is the atomic volume of the rate–controlling diffusing species, L is the grain size, and k is Boltzmann's constant. If it is assumed that the diffusion coefficient of one species is much slower than that of the other,[8] then the effective diffusion constant is given by

$$D_{eff} = D^{\ell} + D^{gb}\pi\lambda / L, \tag{3}$$

where D^{ℓ} is the lattice diffusion coefficient of the slowest–moving species, D^{gb} is the grain–boundary diffusion coefficient, and λ is the grain–boundary width. Equation 3 has neglected pipe diffusion.

If there are multiple diffusion paths, the net fastest path will dominate and D_{eff} will correspond to the slowest–moving species, diffusing by its fastest path.[8] The relationship between point defects and creep can then be derived from

$$D_{eff} = \beta C_v \exp(-Q_m / RT), \tag{4}$$

where β is a constant that contains the jump distance, jump frequency, correlation factor, and a geometrical factor; C_V is the concentration of the point defect that controls creep; and Q_m is the migration energy of the point defect. The concentration of the point defect is determined by the prevailing defect equilibria and is therefore dependent on T, PO_2, and aliovalent impurity or dopant concentration. In the intrinsic region, the functionality of C_V can be included into Eq. 4 to yield

$$\dot{\varepsilon} = B'\sigma[PO_2]^{1/m}\Omega / L^p kT \exp(-Q / RT), \tag{5}$$

where B' is another constant, Q is the activation energy which is the sum of the formation and migration energies, m is the defect signature, and p is the grain–size exponent. The sign and the magnitude of m can be derived from the defect equilibria relationships.

Predictions from the principal viscous creep mechanisms are presented in Table 1, in which Q_{lat} and Q_{gb} represent the lattice and the grain–boundary diffusion activation energies, respectively.[3] A unique viscous creep mechanism cannot be identified solely by measuring the creep parameters Q, n, and p. The creep mechanism can only identified by measurements of the creep parameters as functions of σ, T, and L, combined with careful and detailed microstructural observations. In particular, grain–shape changes and measurements of grain translations and rotations, although often difficult to obtain precisely by techniques such as scanning electron microscopy (SEM), are necessary.

Table 1. Parameters for commonly observed viscous (n = 1) creep mechanisms.

Creep Mechanism	p	Q	Grain–shape Change	Grain Rotation	Threshold Stress
Nabarro–Herring[5,6]	2	Q_{lat}	Yes	No	No
Coble[7]	3	Q_{gb}	Yes	No	No
Ashby–Verall[4]	2	Q_{lat}	No	Yes	Yes
Raj–Ashby[9]	2	Q_{lat}	Yes	No	No

Nonviscous creep mechanisms have also been reported in single crystalline or layered perovskites.[1] In these cases the most commonly cited deformation mechanism is dislocation climb[10] or glide[11] for which p equals zero and the stress exponent becomes 4.5 and 3, respectively. Similarly, the activation energy for climb–controlled dislocation creep is Q_{lat}, while for glide–controlled dislocation creep it becomes Q_{ci}, the chemical interdiffusion coefficient. Creep measurements in these regimes should be combined with transmission electron microscopy (TEM) that focuses on dislocation structures and damage accumulation.

3. CREEP OF POLYCRYSTALLINE $BaTiO_3$

$BaTiO_3$ is an important technical ceramic that finds widespread application as a capacitor. It is surprising, therefore, that little recent work exists on its diffusional properties. Results of compressive creep experiments on polycrystalline $BaTiO_3$ have recently been reported.[12] Measurements were performed over a fairly narrow temperature range, 1200–1300°C, on materials with linear–intercept grain sizes of 19.3–52.4 μm. The narrow temperature range was the result of limited plasticity at the lower temperatures and grain growth at the higher temperatures.

Figure 1 presents normalized strain rate vs. stress for various–grain–sized samples measured at 1300°C at $P_{O_2} = 10^4$ Pa and illustrates several important points. First, the agreement between the two types of experiments, constant–crosshead–velocity and constant–stress, is excellent, which clearly indicates that steady–state deformation was achieved. To determine the creep mechanisms, it is necessary to measure the creep parameters. The solid line has a slope of 1.1 ± 0.2, very close to the value of $n = 1.0$ predicted by any of the viscous creep models. It is also clear that the grain–size exponent is very close to 2.0, which is predicted by the Nararro–Herring or the grain–boundary–sliding creep models.

The measured activation energy was 720 ± 70 kJ/mole. The value of Q measured in the creep study did not agree with the reported activation energies for oxygen diffusion[13] (48 kJ/mole), Ba diffusion[14] (372 kJ/mole), or the 469 kJ/mole reported for creep of single crystals.[15] However, it did agree approximately with the activation energy measured for superplastic flow[16] of fine–grained $BaTiO_3$ and grain growth.[17] It is clear that oxygen diffusion is not responsible for creep. On the other hand, the discrepancies in Q among the Ba tracer–diffusion data, the single–crystal creep data, and the present results were explained by the facts: (1) tracer–diffusion data were obtained on porous samples, and (2) deformation in the single–crystal studies may have been controlled by dislocation glide, not climb. It is believed that the Q measured in compressive creep reflects volume diffusion of the rate–controlling cation. However, no P_{O_2} dependence of $\dot{\varepsilon}$ was found, suggesting

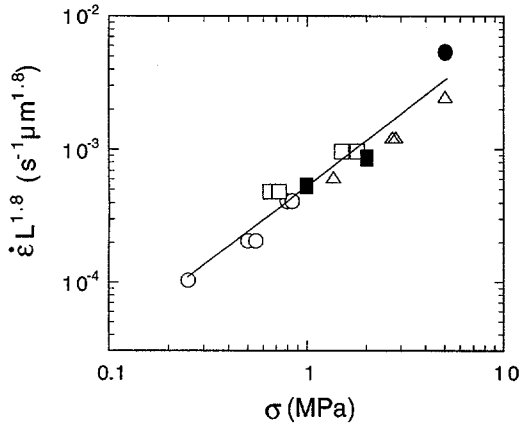

Fig. 1. Plot of normalized strain rate ($\dot{\varepsilon}$ x $L^{1.8}$) vs. steady–state stress for $BaTiO_3$ at 1300°C and P_{O_2} = 10^4 Pa. Open points indicate constant crosshead velocities; closed points indicate constant stress.[12] Circles represent 19.3 μm, squares 30.μm, and triangles 52.4 μm grain sizes.

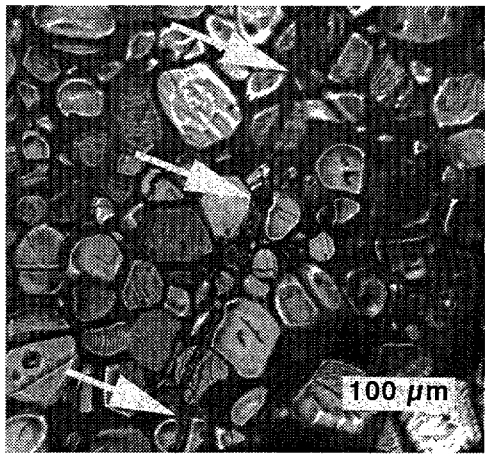

Fig. 2. SEM photomicrograph of 30.9 μm grain–sized $BaTiO_3$ sample after it was deformed at 1300°C and P_{O_2} = 10^4 Pa, showing offsets of initially straight inscribed line, indicated by white arrows and caused by grain–boundary sliding.

that creep was controlled by an extrinsic process.

The discussion above focused on creep parameters, but Table 1 indicates that identification of these parameters is insufficient to specify the deformation mechanism. However, SEM clearly shows that a straight line which was inscribed onto the surface of the sample before deformation has been offset as a result of grain–boundary sliding. The fact that no threshold stress was observed probably means that the Raj–Ashby model best describes the deformation process.[12]

4. CREEP OF $(La_{1-x}Sr_x)_{1-y}MnO_{3+\delta}$

As a result of high electronic and ionic conductivity, LSM materials are attractive for applications such as electrodes and bipolar plates in solid–oxide fuel cells. A comprehensive investigation of compressive creep and its relationship to defect chemistry of LSM has recently been published.[18] Measurement of the creep parameters combined with SEM and TEM allowed one to conclude that grain–boundary sliding accommodated by lattice diffusion was the dominant deformation mechanism.

One of the principal assumptions of the standard defect model for LSM had been that $[V'''_{Mn}]=[V'''_{La}]$, where the brackets indicate concentration and Kroger–Vink notation is used.[18] However, it was clearly shown that the standard defect model could not provide an explanation for the dependence of σ on Sr concentration.[19] The most recent paper explored the P_{O_2} dependence in detail and developed a modified defect model. Key results are shown in Figs. 3 and 4.

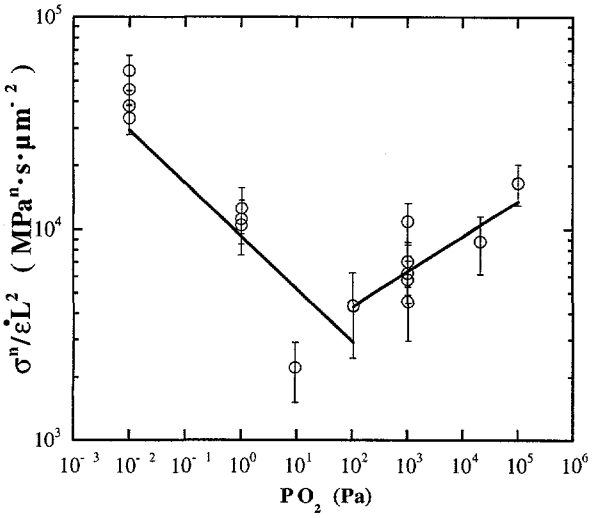

Fig. 3. Normalized stress vs. PO_2 for $La_{0.86}Sr_{0.1}MnO_{3+\delta}$ at 1250°C. The theoretical fit from the cation–vacancy model is shown as a solid line.[18]

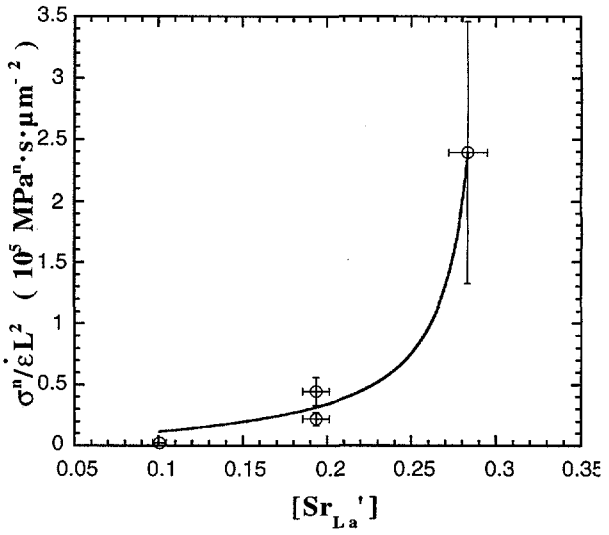

Fig. 4. Normalized stress vs. Sr concentration, with the solid line representing the theoretical fit to the cation–vacancy model (PO_2 = 9.48 Pa and T = 1250°C).[18]

Figure 3 presents the stress normalized by $\dot{\varepsilon}L^2$ vs. PO_2 for the x = 0.1 composition. The lines were calculated from a modified point–defect model that accounted for the A–site deficiency, $[V_{La}'''] = [V_{Mn}'''] + y$, and did not make simplifying assumptions in the electroneutrality relationship. The theoretical and experimental slopes are in reasonable accord. Additionally, the agreement between theory and experiment for the other compositions (x = 0.2 and 0.3) is very good. The model predicts that cation vacancies control creep for lower PO_2, while anion vacancies are the rate–controlling species for higher PO_2. It is also observed that the crossover between cation and anion vacancies moves to higher PO_2 as y decreases. This important result is consistent with the modified defect model and implies that La cations, rather than Mn cations, control creep at the lower PO_2.[18]

The modified defect model may also be used to calculate the $[Sr_{La}']$–dependence of the normalized stress in the same PO_2 regions where it successfully described the PO_2–dependence. These results are shown in Fig. 4, where the reaction constants were adjusted by an unweighted least–squares fit.[18] These kinds of investigations yield information on the minority defects that is not available by other techniques. No cation tracer diffusion data exist to compare to the Q value determined from creep to corroborate the interpretation.

5. CREEP OF LAYERED PEROVSKITES

The compounds Y123, Bi2212, and Bi2223 are now viewed as most likely to be used in superconducting applications.[20] Each is a layered perovskite that has an orthorhombic crystal structure in which the c axis is much longer than either the a

or b axis.[21] The c axis of Y123 is much shorter than that of Bi2212 or Bi2223. In sintered bulk materials, Y123 grains tend to exhibit moderate aspect ratios, whereas Bi2212 and Bi2223 exhibit aspect ratios greater than 10.[22,23] The SFC class of materials has a similar layered–perovskite structure.[24] The grains in most sintered SFC materials also exhibit large aspect ratios (Fig. 5).

Compressive creep data for Y123, Bi2212, and Bi2223 have been reported.[25-32] They will be summarized, along with relevant diffusion data. Emphasis is placed on creep and diffusion measurements made within our programs, in which identical samples were used. The creep data presented on SFC are new. No relevant diffusion data are available.

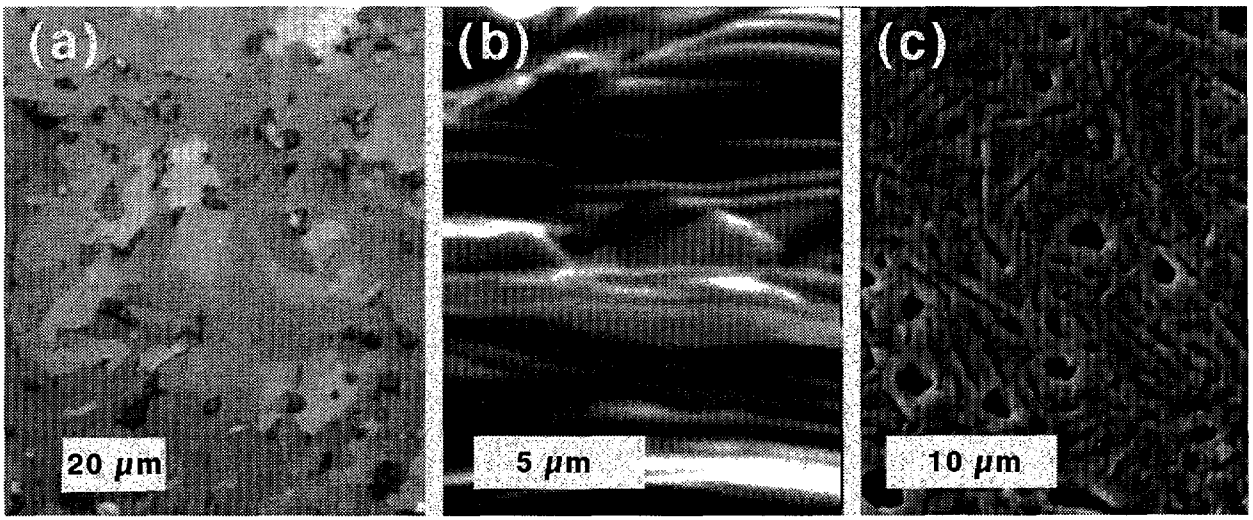

Fig. 5. Representative microstructures of bulk sintered layered perovskites: (a) optical photomicrograph of Y123, in which the grains are randomly oriented,[25] (b) SEM photomicrograph of fracture surface of sinter–forged Bi2212, in which the c axes of the grains are aligned with the forging direction,[23] and (c) SEM photomicrograph of thermally etched surface of SFC, in which elongated grains are approximately randomly oriented.

5.1. Y123

The data set for Y123 is nearly complete (Figs. 6 and 7), in large part because dense, high–quality specimens have been readily available for many years.[25-35] Creep of Y123 occurs by diffusional flow and $n \approx 1$. At T > 0.9 of the melting temperature, lattice diffusion dominates and $Q \approx 1.1$ MJ/mole. At lower temperatures, diffusion along a short–circuiting path, most probably grain boundaries, dominates and $Q \approx 675$ kJ/mole.[27,32] Lower P_{O_2} values decrease the melting point and increase creep rates (Fig. 6).

Essentially no dislocation activity was observed in crept specimens, which is consistent with a diffusional mechanism (Fig. 8a). At $T > 0.9$ of the melting

temperature, the grain–size exponent p was determined to be 2.8 ± 0.6, which could indicate either volume or grain–boundary domination.[25]

The diffusion coefficients of all four constituents of Y123 have been obtained reliably.[26,33-35] Y diffusion was measured with use of rare–earth elements that substitute on the Y site (designated Y* in Fig. 7).[26] Jimenez–Melendo et al. used Eq. 5 to calculate the rate–controlling diffusion coefficient for Y123 creep.[27] With no adjustable parameters, the agreement between the calculation and the values for Y diffusion was excellent (Table 2). The evidence for control of creep rates by diffusion of the A–site cations was clearly established. However, the diffusion rates of Y proved to be too slow to allow for measurement of a PO_2 effect.

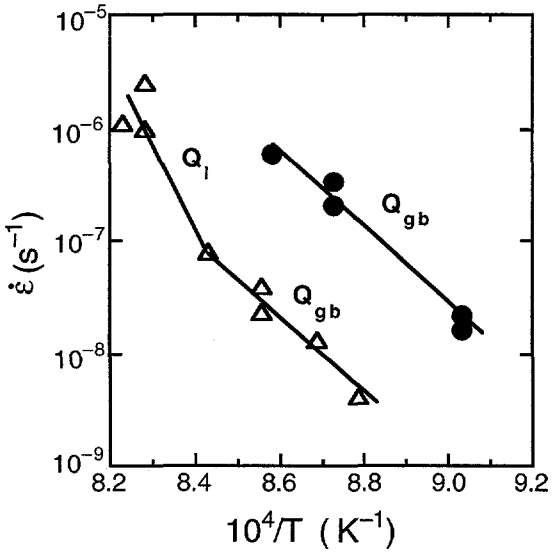

Fig. 6. Strain rate vs. inverse T for Y123, for which lattice diffusion dominates at higher temperature and grain-boundary diffusion at lower temperature; PO_2 = 10^4 Pa (triangles) and PO_2 = 10^3 Pa (filled circles).[27]

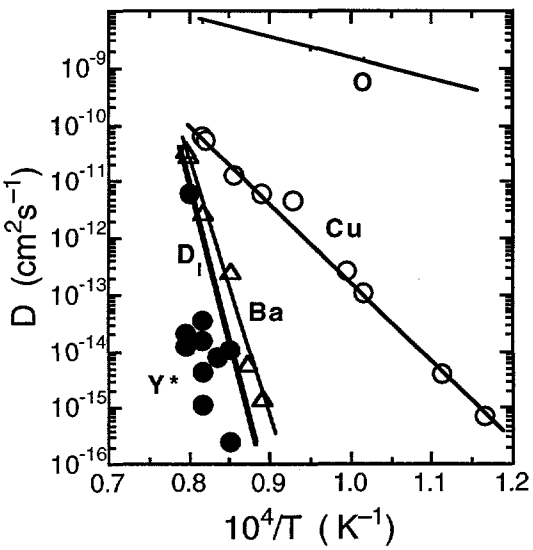

Fig. 7. Diffusion coefficients vs. inverse T for Y123; bold solid line is calculated diffusion coefficient calculated from creep;[27] other diffusion coefficients are labeled and are taken from Refs. 26, 33, 34, and 35.

Table 2. Activation energies obtained in Y123 kinetics studies.

Diffusing species	Q (kJ/mole)	Reference
O	94 ± 3	2,33
Cu	256 ± 4	34,35
Ba	890 ± 80	26
Y	≈1000	26
Creep – lattice	≈1100	27,33
Creep – grain boundary	≈675	27,33

5.2. Bi2212 and Bi2223

Bulk Bi–based high–temperature superconductors are difficult to sinter, and thus various hot–pressing techniques are usually used.[23,36] The resulting specimens exhibit strong textures in which the c axes of the grain are parallel to the pressing direction. Rather surprisingly, creep rates measured in compression have not been found to be dependent on orientation. However, the platelike nature of the grains in Bi2212 and Bi2223 exerts a strong influence on the creep mechanism.[29-31,33] Creep data for these compounds are summarized in Fig. 9.

At very low stresses, Bi2212 deformed by diffusional flow and $n \approx 1$ and Q = 990 ± 190 kJ/mole. At stresses > 20 MPa, $n \geq 3$ and the specimens exhibited small–scale fracturing and significant dislocation activity. It was concluded that steady–state creep had occurred only for stresses < 10 MPa.[29,30] The creep rates of Bi2223 were nearly equal to those of Bi2212, but $n \approx 3$ for all measured stresses.[30,31] Significant dislocation activity, with little cracking, was observed. It was concluded that steady–state deformation by a dislocation–climb mechanism had been established and that the measured activation energy of 1000 ± 80 kJ/mole reflected diffusion of one of the A–site cations.[31]

Reliable diffusion data exist for O[37] and a surrogate for Cu[38] in Bi–2212 and for Sr[39] in Bi2212 and Bi2223. The respective activation energies of 90 ± 3, 181 ± 5, 553 ± 34, and 519 ± 130 kJ/mole are far lower than those measured in creep. Other data[40] for Bi2212 and comparison with data from Y123 suggest that lattice diffusion of Ca or possibly Bi controls the creep rate.[31] The high activation energies for creep are approximately equal to those obtained from phase–transformation studies.[41]

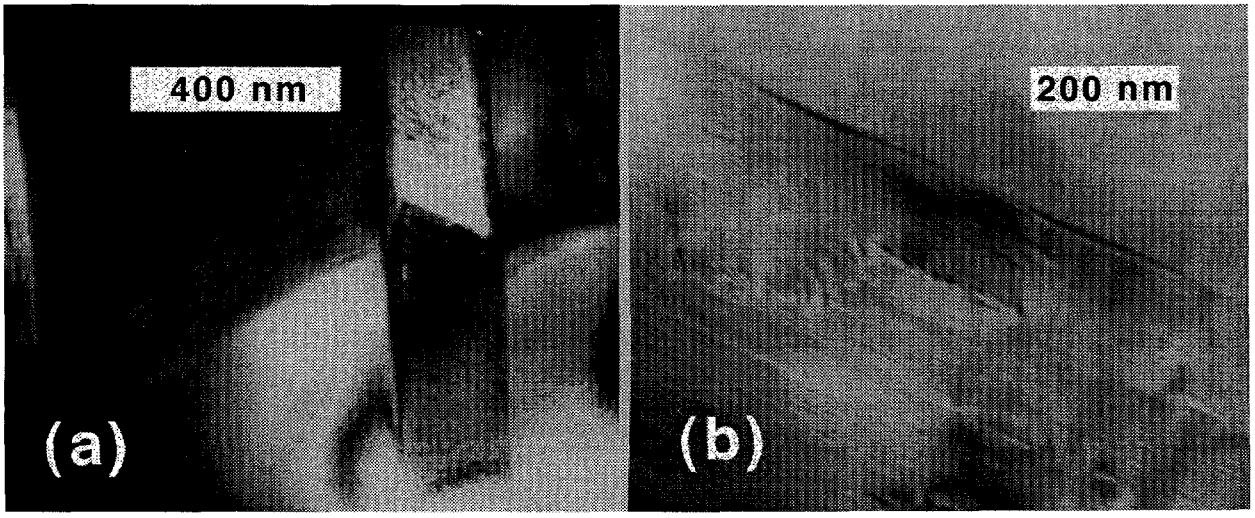

Fig. 8. TEM photomicrographs of layered perovskite specimens after creep testing: (a) Y123, in which few dislocations are observed, and (b) SFC in which glide dislocations are observed.

5.3. SCF

SFC powder of composition $SrFe_{1.2}Co_{0.3}O_x$ was made by reaction of $SrCO_3$, Fe_2O_3, and $Co(NO_3)_2 \cdot 6H_2O$. Pellets were made by cold–pressing at 120 MPa and then sintering in air at 1200°C for 5 h, resulting in >90% dense materials.[24] Right parallelepipeds ≈6 x 3 x 3 mm were cut from the pellets. The 3 x 3 mm compression surfaces were polished flat and parallel. The samples were deformed at constant load in air at 940 and 1000°C. It is planned to study the dependence of SFC creep on σ, PO_2, and T; to date, we have acquired preliminary data only (Fig. 10). However, these data fit well with those of the other layered perovskites.

At low stresses, SFC deformed by diffusional flow and $n \approx 1$ and at higher stresses, dislocation activity was significant (Fig. 8b) and $n \approx 3$. The dislocation structures were consistent with a glide–controlled process rather than the type of climb control evinced by Bi2223. It is clear that at high stress grains with large aspect ratios tend to deform by dislocation motion. Future work with SFC will focus on completing the data set and calculations of diffusion rates. Given the effort worldwide in SFC–type oxides, it is likely that at least some diffusion data should be available soon to compare with these calculations.

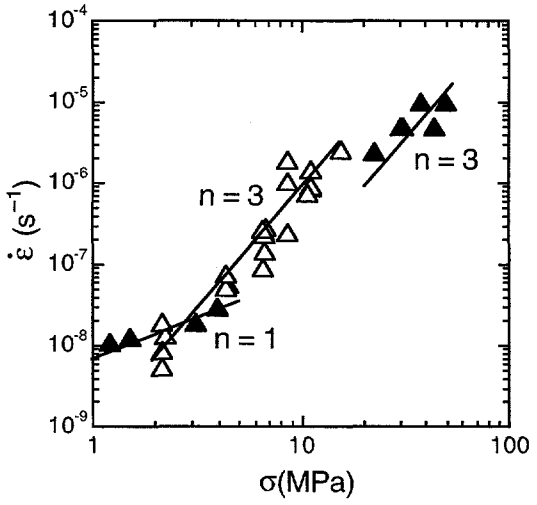

Fig. 9. Strain rate vs. stress for Bi2212 (filled triangles) and Bi2223 (open triangles) in air at 800°C; stress exponents are shown.[29-31]

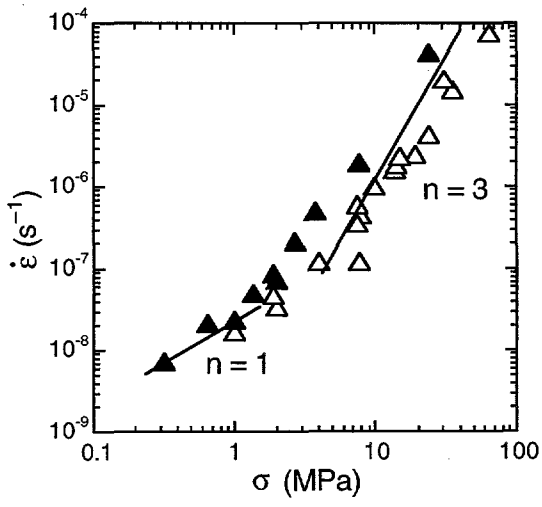

Fig. 10. Strain rate vs. stress for SFC in air at 940°C (open triangles) and 1000°C (filled triangles); stress exponents are shown.

6. SUMMARY

We have demonstrated that measurements of steady–state creep combined with careful microstructural observations can be used to identify deformation mechanisms, providing examples from studies of perovskite–structured electronic ceramics. Most commonly found deformation mechanisms are linked to the defect

chemistry of the minority species. Additionally, once the mechanism has been identified, the creep measurements can be used to calculate the diffusion coefficient of the rate–controlling species. While it is not always clear whether the A– or B–site cation in perovskites is the controlling species, the results nevertheless can serve as a check on the diffusion constants measured by other techniques. Diffusion data obtained from creep experiments can be used to understand and control processes, such as sintering, which are also controlled by diffusion of the slowest–moving species.

ACKNOWLEDGMENTS

The authors are grateful to Drs. R. E. Cook, A. Domínguez–Rodríguez, J. Martínez-Fernandez, J. Jimenez–Melendo, E. T. Park, and J. Wolfenstine for their diligent work and many helpful discussions. The LSM samples were provided by Dr. T. R. Armstrong and the SFC materials were provided by Dr. B. Ma.

REFERENCES

1) A. Domínguez–Rodríguez, M. Jiménez–Melendo, N. Chen, K. C. Goretta, S. J. Rothman, and J. L. Routbort, J. Phys. III France **4** (1994) 253.

2) J. L. Routbort and S. J. Rothman, J. Appl. Phys. **76** (1994) 5615.

3) W. R. Cannon and T. G. Langdon, J. Mater. Sci. **18**, (1983) 1.

4) M. F. Ashby and R. A. Verrall, Acta Metall. **21** (1973) 149.

5) F. R. N. Nabarro, in: Report of a Conference on Strength of Solids, The Physical Society, London, 1950, p. 75.

6) C. Herring, J. Appl. Phys. **21** (1950) 437.

7) R. L. Coble, J. Appl. Phys. **34** (1963) 1679.

8) M. Jiménez, A. Domínguez-Rodríguez, R. Márquez, and J. Castaing, Phil. Mag. **56** (1987) 767.

9) R. Raj and M. F. Ashby, Metall. Trans. **2** (1971) 1113.

10) J. Weertman, J. Appl. Phys. **28** (1957) 362.

11) J. Weertman, J. Appl. Phys. **28** (1957) 1185.

12) E. T. Park, P. Nash, J. Wolfenstine, K. C. Goretta, and J. L. Routbort, J. Mater. Res. **14** (1999), 523.

13) J. Doskocil, Z. Pospisil Silikaty **16** (1976) 113.

14) A. G. Verduch and R. Lindner, Arkiv. Kemi. **5** (1953) 313.

15) S. Beauchesne and J. P. Poirier, Phys. Earth Planet Inter. **55** (1989) 187.

16) C. Carry and A. Mocellin, J. Am. Ceram. Soc. **69** (1986) C215.

17) E. T. Park, J. Mater. Sci. **18** (1999) 163.

18) R. E. Cook, K. C. Goretta, J. Wolfenstine, P. Nash, and J. L. Routbort, Acta Mater. **47** (1999) 2969.

19) J. Wolfenstine, K. C. Goretta, R. E. Cook, and J. L. Routbort, Sol. State Ion. **92** (1996) 75.
20) See, e.g., U. Balachandran and A. N. Iyer, Mater. Technol. **11**(1996) 145.
21) C. Park and R. L. Snyder, J. Am. Ceram. Soc. **78** (1995) 3171.
22) S. Jin and J. E. Graebner, Mater. Sci. Eng. **B7** (1991) 243.
23) C.–Y. Chu, J. L. Routbort, N. Chen, A. C. Biondo, D. S. Kupperman, and K. C. Goretta, Supercond. Sci. Technol. **5** (1992) 306.
24) B. Ma, J. P. Hodges, J. D. Jorgensen, D. J. Miller, J. W. Richardson Jr., and U. Balachandran, J. Sol. State Chem. **141**(1998) 576.
25) K. C. Goretta, J. L. Routbort, A. C. Biondo, Y. Gao, A. R. de Arellano–López, and A. Domínguez–Rodríguez, J. Mater. Res. **5** (1990) 2766.
26) N. Chen, J. L. Routbort, S. J. Rothman. and K. C. Goretta, J. Mater. Res. **7** (1992) 2308.
27) J. Jimenez–Melendo, A. R. de Arellano–López, A. Domínguez–Rodríguez, K. C. Goretta, and J. L. Routbort, Acta Metall. Mater. **43** (1995) 2429.
28) J. Jimenez–Melendo, A. Domínguez–Rodríguez, and J. L. Routbort, Scripta Metall. Mater. **32** (1995) 621.
29) J. L. Routbort, K. C. Goretta, D. J. Miller, D. B. Kazelas, C. Clauss, and A. Domínguez–Rodríguez, J. Mater. Res. **7** (1992) 2360.
30) K. C. Goretta, E. J. Zamirowski, J. M. Calderón–Moreno, D. J. Miller, N. Chen, T. G. Holesinger, and J. L. Routbort, J. Mater. Res. **9** (1994) 541.
31) J. Martínez-Fernandez, A. Domínguez-Rodríguez, J. L. Routbort, and K. C. Goretta, Scripta Mater., in press (2000).
32) P. E. Reyes–Morel, X. Wu, and I.–W. Chen, in *Ceramic Superconductors II*, ed. M. F. Yan (Am. Ceram. Soc., Westerville, OH, 1989) p. 590.
33) S. J. Rothman, J. L. Routbort, U. Welp, and J. E. Baker, Phys. Rev B **44** (1991) 2326.
34) D. Gupta, R. B. Laibowitz, and J. A. Lacey, Phys. Rev. Lett. **64** (1990) 2675.
35) J. L. Routbort, S. J. Rothman, N. Chen, J. N. Mundy, and J. E. Baker, Phys. Rev. B **43** (1991) 5489.
36) K. C. Goretta et al., Appl. Supercond. **2** (1994) 411.
37) M. Runde, J. L. Routbort, S. J. Rothman, K. C. Goretta, J. N. Mundy, X. Xu, and J. E. Baker, Phys. Rev. B **45** (1992) 7375.
38) Y Fang, S. Danyluk, K. C. Goretta, N. Chen, M. Runde, S. J. Rothman, and J. L. Routbort, Appl. Phys. Lett. **60** (1992) 2291.
39) N. Chen, S, J. Rothman, and J. L. Routbort, J. Mater. Res. **8** (1993) 2465.
40) M. V. Slinkina, L. I. Volosentseva, G. I. Dontsov, A. S. Zhukovskaya, and A. A. Fotiev, Supercond. **5** (1992) 1819.
41) W. Zhu, C. K. Kuo, and P. S. Nicholson, J. Mater. Res. **14**(1999) 4143.